metals

MDPI

Article

Failure Analysis of Hydraulic Expanding Assembled Camshafts Using BP Neural Network and Failure Tree Theory

Jianping Ma, Lianfa Yang *, Lin Song, Zhiwei Gao, Saisai Pang and Haimei Han

School of Mechanical and Electrical Engineering, Guilin University of Electronic Technology, Guilin 541005, China
* Correspondence: y-lianfa@163.com

Abstract: Due to the complex and changeable working environment of assembled camshafts using tube hydroforming (THF) technology, the manifestations of failure, the causes of failure and the preventive measures for these failures are a major concern. Therefore, in view of this new connection technology for assembled camshafts, it is important to put forward a prediction and evaluation method of failure for hydraulic expanding assembled camshafts. In this study, an isometric-trilateral profile cam was used to complete the hydroforming connection with the hollow shaft (tube) under different hydraulic pressures. Orthogonal torsion experiment and laser measurement experiment were performed. Finite element analysis was carried out using ABAQUS 6.14 software, and relevant research data were obtained. A more accurate BP neural network model was constructed to predict the main failure factors of assembled camshafts. The failure manifestations of assembled camshafts are displayed by the experiment from the microscopic perspective. The causes of failure are analyzed by using the minimum cut set in the failure Tree (FT) theory. The effect of basic causes on the subsystems is analyzed, and the weight distribution of the main events in the FT is given. Finally, the specific measures to prevent failure are proposed from a macro perspective. The research is of great significance to study the failures of assembled camshafts in service to further the production, manufacturing, failure prevention, faults monitoring and performance improvement of assembled camshafts in the engine industry.

Keywords: assembled camshaft; failure manifestations; hydraulic expanding; BP neural network; failure tree

Citation: Ma, J.; Yang, L.; Song, L.; Gao, Z.; Pang, S.; Han, H. Failure Analysis of Hydraulic Expanding Assembled Camshafts Using BP Neural Network and Failure Tree Theory. *Metals* **2022**, *12*, 1639. https://doi.org/10.3390/met12101639

Academic Editor: João Manuel R. S. Tavares

Received: 24 August 2022
Accepted: 27 September 2022
Published: 29 September 2022

1. Introduction

Camshafts are mainly composed of spindle, cam and journal, which is the key part of the valve drive group in the engine valve train [1]. The manufacturing process of traditional camshafts is mainly one-piece casting or forging. The materials of all parts are the same, which makes it difficult to meet the performance requirements of different parts. There are problems such as heavy weight and low manufacturing precision. Assembled camshafts combine different parts (shaft, cam, journal, etc.) separated and manufactured according to different performance requirements to better exert the performance of different materials. Among them, hollow shaft can effectively reduce the overall quality of camshafts, which has significant advantages in large-scale and lightweight production in the automobile industry [2]. Therefore, the assembled camshaft has a broad development prospect in automobiles, railways, heavy military vehicles, warships, marine engines and other fields [3,4].

According to the literature [5], the connection methods of assembled camshafts mainly include: hydroforming technology, interference fit technology and bonding technology. Tube hydroforming (THF) is a competitive hollow part forming technology and a camshaft assembly technology with broad prospects [6,7]. That is, the shaft is bulged under the hydraulic pressure and axial force and finally press-fitted on the cam hole to achieve connection. Through the assembled camshaft after hydraulic expanding, a mechanical

mutual embedded expanding structure is formed at the expanding interface between the cam and the shaft. However, with the continuous improvement of the power and torque speed of the engine, when the camshaft is required to transmit large torque, this stable interface state may be difficult to maintain. In light cases, vibration, impact, etc., occur, affecting the transmission accuracy and stability. At worst, it causes the separation between the cam and the shaft, resulting in the failure of the camshaft. Therefore, it is of great significance to analyze the failures of assembled camshafts as a service to the production and manufacturing of camshafts, failure prevention and fault monitoring in the engine industry. At present, most scholars have predicted and studied the failure, fatigue, fault and life of engine camshafts or crankshafts and have achieved a series of research results.

First, many scholars have carried on the related research by using the experimental method. Zhang et al. [8] carried out uniaxial and multi-axial low cycle fatigue tests on hollow cylindrical butt joints bonded with automobile sealant under the stress control mode; analyzed the effects of equivalent stress amplitude, equivalent average stress and loading frequency on the fatigue life of the specimens and proposed a comprehensive consideration of the effects of loading path, equivalent stress amplitude, equivalent average stress and loading frequency on multi-axial fatigue life. The results show that the improved fatigue life prediction model can better predict the multi-axial fatigue life of bonded butt joints. Yanarocak et al. [9] introduced the synchronous design and development work of the diesel engine valve system, solved the problems of installing instruments on the quick lubrication system running at about 140 °C and selecting the appropriate position that can reflect the correct stress, and eliminated the risk of catastrophic failure of valve control system and related engine components through optimization research and verification process. Singh et al. [10] summarized the fatigue failure mechanism of automobile crankshaft under working loading from a random point of view. In this study, the fatigue failure of crankshafts is summarized; the random method is discussed by using the empirical model, and the safety life method is used to evaluate the random fatigue failure and damage. Ktari et al. [11] studied the failure by means of SEM, fracture analysis and tensile and hardness experiments. To further strengthen this point, Becerra et al. [12] analyzed the failure through chemical analysis, X-ray analysis and visual technology. Liu et al. [13] and Ling et al. [14] monitored the random fatigue damage model under variable amplitude loading, which provided an important index for durability evaluation. To evaluate the fatigue properties of metals, Jeon et al. [15] developed a practical expert system to predict the fatigue properties of metals. It is possible to predict the life of materials by fatigue, but this is only limited to the actual loading process of components from the experimental analysis.

Next, some scholars use the method of combining experiment and simulation to carry out relevant research. Wang et al. [16] tested the camshaft made of gray cast iron under cyclic bending and torsion, simulated it with the finite element method and proposed a new crack simulation technology to predict the fatigue limit. Ossai et al. [17] proposed a random method, which can generate random and nearly similar data experimental results and predict the fatigue life cycle or imminent fatigue damage by deterministic and stochastic methods. In a random process, the loading data are converted into equal time steps using the relevant continuous or discrete time. Meanwhile, the statistical root mean square error and other parameters are used to test the data divergence level and the accuracy of failure in the random model. Nipane [18] performed finite element modeling and failure analysis for standard gray cast iron camshafts and composite camshafts through Pro-E 4.0 and ANSYS Workbench 11.0 software. The results show that the fatigue life of composite camshafts is better than that of cast iron camshafts. Zhai et al. [19,20] designed two new types of camshaft mating surface structures, i.e., isometric-trilateral profile and logarithmic spiral, measured the contact clearance and contact length between the shaft and the cam through the finite element method to reflect the connection strength, and developed the experiment verification, but did not investigate related failure of the assembled camshaft. Qiao et al. [21] simulated and analyzed the assembly process of the knurled connection

camshaft, discussed the equivalent stress at different torsional moments, and tested the static torsion strength. It was found that when there is angular displacement (accuracy is 0.7 degrees) between cam and shaft, the torque is regarded as the static torsion strength, which meets the actual working requirements of camshaft through verification and proves that the assembly has certain reliability. Londhe et al. [22] established a spatial model of the valve mechanism of a four-stroke engine and established a camshaft model based on hydroforming. The contact stress between the cam and the push rod in the high-speed rotating camshaft was analyzed, and it was found that the camshaft can withstand the impact force brought by the push rod when there is torsion at high speed. Moreover, the fatigue coefficient of camshafts is discussed.

Finally, some scholars adopt the theory of optimization algorithm and deep learning to develop a series of research. Dong et al. [23] used the K-means clustering algorithm to select the clustering center of radial basis function neural network for camshaft grinder, the key equipment of camshaft production line, and proposed a fault prediction model based on RBF neural network. The results show that the distribution density is 1, and the approximation error of the neural network is more reasonable. The application of the model is illustrated by an industrial example, which proves that the proposed method is effective. Yang [24] developed to apply the Drosophila optimization algorithm to the multivariable process fault diagnosis model and analyzed the out-of-control sample data in automobile crankshaft production. Li et al. [25] proposed a fault diagnosis method based on manifold learning and swarm intelligence optimization. Firstly, three manifold learning algorithms are used to fuse the features extracted from the original vibration data of diesel engine into a new nonlinear space. Secondly, a multi class multi kernel correlation vector machine optimized by swarm intelligence is proposed, and the fault is identified by using the fusion features. Subsequently, the comprehensive advantages of multi-core function and weighting strategy are used to realize the fault detection of diesel engine. Finally, the experimental data of a commercial diesel engine verify the effectiveness of this method herein.

However, most of the above studies have been carried out through experimental research, numerical analysis and related optimization algorithm and achieved certain results, but some studies lack quantitative analysis. In addition, for the novel structure of assembled camshafts using hydraulic expanding technology, failure research is affected by many factors, and some parameters are not easy to obtain. There are some difficulties in the determination, prediction and analysis of failures for the assembled camshaft. Therefore, the cam with isometric-trilateral profile is selected to connection with hollow shaft (tube) under different hydraulic pressure. The orthogonal torsion experiment and laser measurement experiment under different parameters are performed; ABAQUS 6.14 software is used to carry on the finite element simulation, and the related data are obtained. The BP neural network model is established, and the main failure factors are determined and predicted. Then, the failure manifestations of assembled camshafts are displayed. The causes of failure are analyzed by using the minimum cut set in the failure tree (FT) theory. Finally, the specific measures to prevent failure are proposed in this study.

This paper is organized as follows. The introduction is presented in Section 1. The experimental research, including hydraulic expanding experiment, orthogonal torsion experiment and laser measurement experiment, is provided in Section 2. The finite element analysis, including the establishment of a finite element model and relevant parameters settings, is given in Section 3. The BP neural network model is established in Section 4. The results and discussion, which are prediction result and error analysis of failure factors using BP neural network, the failure manifestations of assembled camshaft, the calculation of FT minimum cut set to analyze the cause of failure of the assembled camshafts and the specific measures to prevent failure, are showed in Section 5. Finally, the main conclusions are highlighted in Section 6.

2. Experimental Research

This study mainly includes three parts of the experiment. The first part is the hydraulic expanding experiment, namely, the cam and the tube are assembled under different hydraulic pressures. The second part is the orthogonal torsion experiment under different parameters which is carried out for the camshaft after the expansion. The purpose is to obtain a sufficient amount of experimental data for the training of the BP neural network to obtain a higher-precision training model. The final part is the laser measurement experiment, which is used to obtain the parameters (i.e., the main failure factors) that cannot be directly measured in the orthogonal torsion experiment.

2.1. Description of Structure and Materials

The assembled camshaft was formed by connecting the shaft with the inner hole of the cam. However, the inner hole profile of the cam affects the torsion strength of the assembled camshaft. In recent years, some scholars have shown that the inner hole profile of the cam can be made into a non-circular structure. Some non-circular structures include isometric-trilateral [26], logarithmic spirals [20], sinusoids and cycloids. In this study, the isometric-trilateral profile structure was selected as the inner hole profile of the cam, as shown in Figure 1a. The isometric-trilateral profile can be expressed as [27].

$$x(\alpha) = (D_i/2 + e)\cos\alpha - e\cos n\alpha\cos\alpha - ne\sin n\alpha\sin\alpha \quad (1)$$

$$y(\alpha) = (D_i/2 + e)\sin\alpha - e\cos n\alpha\sin\alpha + ne\sin n\alpha\cos\alpha \quad (2)$$

where D_i is the diameter of the small circle, n is the number of polygon sides (n = 3 in this study), and e is the offset distance, which determines the shape of the profile. In addition, α is the angle formed by a certain point on the function curve in the rectangular coordinate system. According to the properties of the curve, the curve is composed of three arcs FB, BD, and DF and is symmetrical about the segments AD, CF, and EB, respectively. The diameter of the big circle can be calculated as follows:

$$De = (D_i + 4e) \quad (3)$$

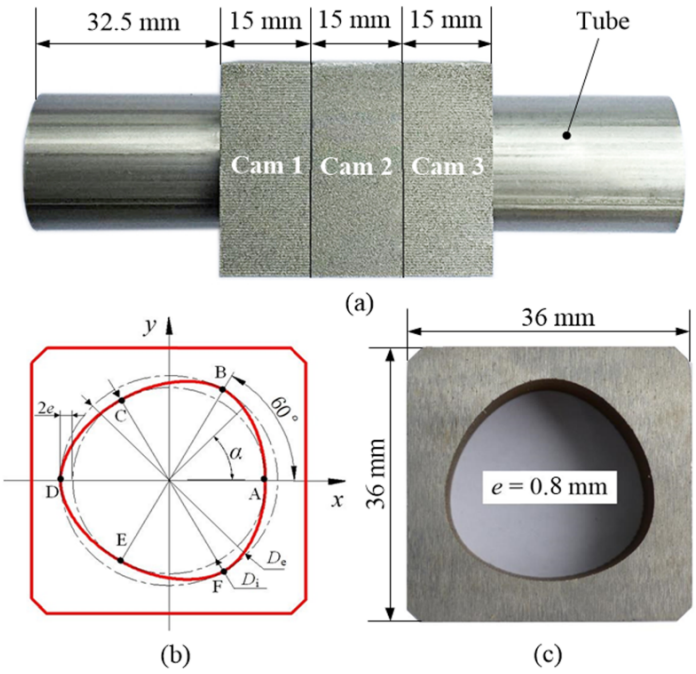

Figure 1. (**a**) Schematic of the assembled camshaft, (**b**) schematic of the isometric-trilateral profile of the cam and (**c**) actual image of the cam [28].

The outer shape of the cam was designed as a square structure with a length of 36 mm (Figure 1c). To facilitate the subsequent analysis, three identical cams with a thickness of 15 mm were designed in this study (Figure 1a). The diameters D_i and D_e of the small and big circles were 25.3 and 28.5 mm, respectively (Figure 1b), and the offset distance e of the cam was 0.8 mm. The length, diameter and wall thickness of the tube were 110, 25 and 0.6 mm, respectively. The materials of the tube and cam were SUS304 stainless steel and 45 steel, respectively. The chemical composition of the two materials is listed in Table 1. Table 2 presents the material mechanical parameters of the tube and the cam.

Table 1. Chemical composition of SUS304 tube and 45 steel cam (wt.%).

Part	Fe	C	Si	Mn	P	S	Cr	Ni	Cu	Al
Tube	Base	0.07	0.47	1.94	0.028	0.001	16.59	8.29	—	1.05
Cam	Base	0.45	0.27	0.65	—	—	0.18	0.2	0.2	—

Table 2. Mechanical properties of SUS304 tube and 45 steel cam.

Part	Young's Modulus E/GPa	Poisson Ratio μ	Yield Strength σ_y/MPa	Tensile Strength σ_b/MPa
Tube	215	0.285	423	1466
Cam	203	0.269	355	660

2.2. Experimental Details

2.2.1. Hydraulic Expanding Experiment

The connection experiments were performed on a hydraulic machine with a CNC system (YB98-200A from Guangdong Sihao Hydraulic Technology Co., Ltd., Foshan, Guangdong, China), as shown in Figure 2a. The connection of the camshaft is mainly completed by the main cylinder, the left and right stamping cylinders, the control panel, the hydraulic pump, the pressurized cylinder, the left and right punches and the THF die. The punches are installed on the left and right stamping cylinders, and the stamping cylinders realize left and right synchronized feed movement of the punches. The purpose is to provide sealing to both ends of the tube. The hydraulic pump (4DSY-22/60 from Shenmo Electric Co., Ltd., Shanghai, China) and the pressurized cylinder provide hydraulic pressure for the camshaft connection test. The inside of the tube is filled with fluid through the left punch hole, causing the tube to plastically deform. Hydraulic pressure is applied by the control panel, which also applies variation of hydraulic pressure with time. In the hydroforming system, the rated maximum hydraulic pressure is 85 MPa. The synchronization accuracy of the left and right stamping cylinders is not greater than 0.1 mm. The THF principle of the equipment is demonstrated in Figure 2b. First, the cam and tube are placed and fixed between the upper and bottom dies. Second, the upper and lower dies are clamped by the pressure of the main cylinder to fix the cam and the tube. Third, the left and right punches move the left and right to provide sealing to the ends of the tube, filling the tube with fluid through the left punch hole to provide hydraulic pressure. Finally, the cam and tube are assembled under different hydraulic pressures.

The hydraulic pressures used in this experiment are 65, 70, 75 and 80 MPa, respectively. Since the linear loading mode of hydraulic parameters is easy to control compared with other broken line loading modes on the equipment, the loading curve is not easy to shake. Therefore, the hydraulic parameters in this study are linearly loaded to ensure the expanding performance of the assembled camshafts.

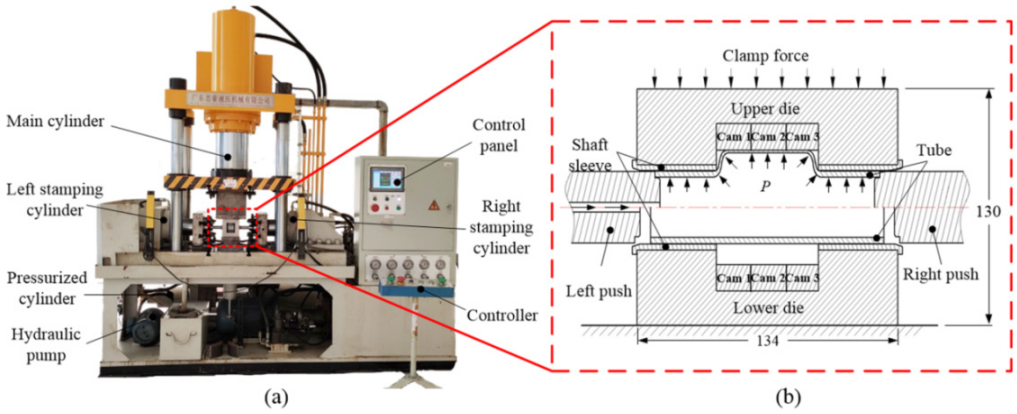

Figure 2. (**a**) CNC tube hydroforming system YB98-200A and (**b**) the connection principle of the assembled camshaft [29].

2.2.2. Orthogonal Torsion Experiment

The equipment used for orthogonal torsion experiment of camshaft is TTM502-A1 electronic torsion test rig produced by Shenzhen Sansi Zongheng Technology Co., Ltd. (Shenzhen, Guangdong, China), as shown in Figure 3a. The measuring range of the torque is 1–100% FS (full scale). The relative error of the torque, torsion angle and torsion angle of the torsion meter are ±0.5%, ±1.0%, and ±1.0%, respectively. The torsion velocity range is 4–720 °/min, and the relative error of the torsion velocity is within ±1.0% of the set value. This can be used for torsion performance experiment on metal materials, non-metallic materials, composite materials and components. Since the camshaft in this study is a hollow structure, considering the installation problem, a set of torsion fixtures is self-designed, as demonstrated in Figure 3b. During this torsion experiment, cams 1 and 3 were fixed, cam 2 was torqued, and the torsion strengths between cam 2 and tube were obtained and recorded in real-time using the computer acquisition software.

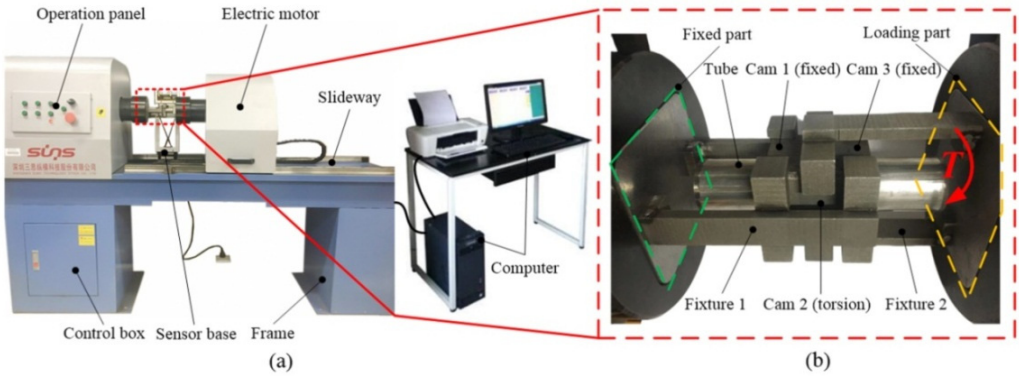

Figure 3. Orthogonal torsion experiment equipment for assembled camshafts [28]: (**a**) TTM502-A1 electronic torsion test rig and (**b**) detailed view.

By changing the maximum expanding hydraulic pressure, torsion velocity and maximum torsion angle, the torsion orthogonal experiment with three factors and four levels is carried out. The specific system parameters are listed in Table 3. With the aid of professional experimental design software Design_expert_8, the optimal design method in response surface design is adopted, and the quadratic model is selected for three-factor four-level orthogonal experimental design. Finally, 20 sets of experimental schemes were obtained, as displayed in Table 4. The experimental scheme not only avoids the heavy experiment task but also considers the influence of multiple system parameters on the experimental results, which is more reasonable and effective. Furthermore, repeated experiments were performed to verify the repeatability of the experiment.

Table 3. Factors and levels of orthogonal torsion experiment.

Factors	Level 1	Level 2	Level 3	Level 4
Maximum hydraulic pressure P_{max}/(MPa)	65	70	75	80
Torsion velocity v/(°/min)	4	5	6	7
Torsion angle a/(°)	6	7	8	9

Table 4. Orthogonal torsion experiment scheme (input value of BP neural network).

No.	Torsion Velocity v/(°/min)	Maximum Hydraulic Pressure P_{max}/(MPa)	Torsion Angle a/(°)
1	4	65	6
2	4	65	9
3	4	75	7
4	4	80	8
5	5	70	7
6	5	70	7
7	5	75	9
8	5	75	9
9	5	80	6
10	5	80	6
11	6	65	8
12	6	65	8
13	6	70	7
14	6	70	7
15	6	80	9
16	7	65	6
17	7	70	9
18	7	75	6
19	7	80	8
20	7	80	8

Through the above-mentioned 20 sets of orthogonal torsion experiments, the torque values listed in Table 5 were measured. In addition, the drawings of assembled camshafts before and after torsion are shown in Figure 4.

Table 5. Main failure factors of assembled camshaft (output value of BP neural network).

No.	Torque T/(N·m)	Surface Roughness R_q	Scratch width b_{avg}/(um)	Shear Stress τ/(MPa)	Residual Contact Pressure P_n/(MPa)
1	21.4145	1.306	14.256	15.9366	170.099
2	30.7890	3.951	46.329	20.6680	179.326
3	20.2384	1.842	12.753	6.2725	82.904
4	25.9765	0.958	23.699	17.9093	207.934
5	23.6245	1.306	25.124	13.7821	138.834
6	18.9849	1.236	19.169	13.4588	133.252
7	29.5700	2.557	45.238	7.7986	83.071
8	31.2356	2.311	52.733	8.2564	83.297
9	18.3333	0.627	15.530	18.7162	203.519
10	19.4047	1.891	15.223	18.3961	206.802
11	25.4813	1.817	26.871	12.2360	168.744
12	27.6493	2.472	28.036	11.7208	170.439
13	17.9282	2.264	16.497	8.5697	139.241
14	21.0662	2.015	24.326	9.3190	142.312
15	31.5135	1.391	47.229	17.5566	207.925
16	19.4324	2.786	27.049	13.4096	170.256
17	20.4762	3.467	25.637	8.7113	139.929
18	25.9765	1.573	37.125	10.4553	95.032
19	25.9894	1.478	36.758	17.6845	206.519
20	26.1291	1.633	39.146	18.1240	202.168

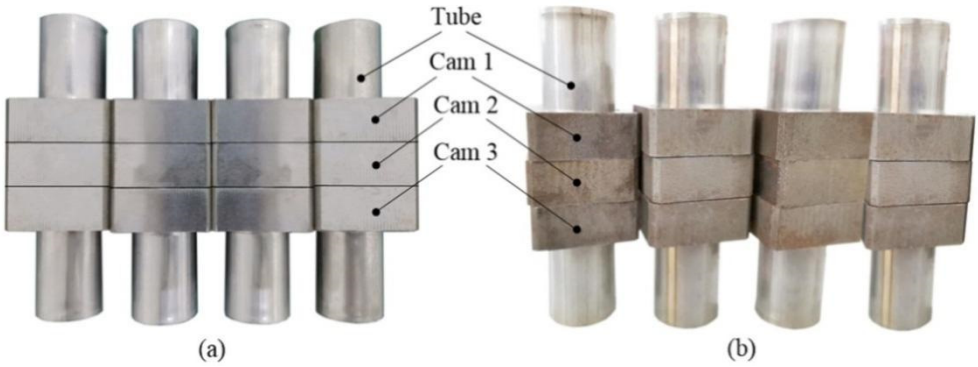

Figure 4. Drawing of a partially assembled camshaft [28]: (**a**) before torsion and (**b**) after torsion.

2.2.3. Laser Measurement Experiment

After the orthogonal torsion experiment, the drawings of assembled camshafts as shown in Figure 4b are obtained. Since the failure modes we proposed, including tubular surface roughness and scratch width, are not easy to measure directly in torsion experiment, it is necessary to use an OLYMPUS OLS4100 3D measuring laser microscope for measurement, as illustrated in Figure 5a. The equipment is a high-precision technology product of Olympus Co., Ltd., of Tokyo, Japan. It has two sets of optical systems for information collection, namely, an optical system for obtaining color information of samples and a laser confocal optics for measuring irregularities on the sample surface, with a resolution of 1 nm and a measurement accuracy of ±1.5%. The microscopic profile and 3D shape of the parts can be measured, including the surface topography, length and width, height, volume and surface roughness.

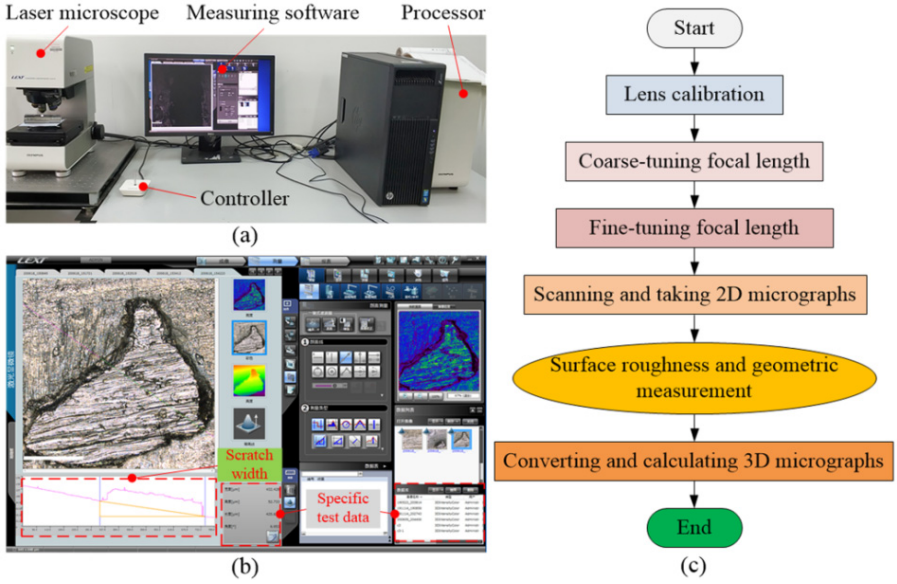

Figure 5. OLYMPUS OLS4100 3D measuring laser microscope: (**a**) system composition, (**b**) measurement interface and (**c**) measurement procedure.

The main measurement procedure is displayed in Figure 5c, including the following processes: First, the focal length of the micro lens is roughly adjusted. The measuring surface of the tube is placed in the middle of the stage. The lens is aligned with the measurement area by mouse and controller. Then, the focal length of the instrument lens is fine-tuned by adjusting the mouse wheel until the outline is clear, so as to obtain a clear focal length range. Subsequently, the appropriate focal length is selected and the measurement button is clicked. The system scans and calculates the sample contour through the microscope lens. According to the obtained two-dimensional micrograph,

the surface roughness and geometric measurement buttons are clicked, respectively, the appropriate area to calculate the surface roughness and scratch width is selected, and finally the relevant data are obtained as listed in Table 5. To reduce measurement error, scanning, measurement and calculation are carried out three times on the tubular outer surface at the same position. Finally, to obtain better morphology, the 2D micrograph is converted into 3D morphology. The measurement software interface is shown in Figure 5b.

3. Finite Element Analysis

Because the individual parameters and samples required by the BP neural network cannot be directly obtained from the above experiments, the purpose of this finite element analysis (FEA) is to extract the residual contact pressure and shear stress values for building an accurate BP neural network model. The FE model of hydraulic expanding assembled camshaft is established using ABAQUS 6.14 software, as shown in Figure 6a, which mainly includes four parts: cam, tube, left die and right die. The structure, materials and process parameters are consistent with the above experiment. For example, the hydraulic pressure is 65, 70, 75 and 80 MPa, and the loading path adopts linear loading and is consistent with the above experiments, as presented in Figure 7. Two analysis steps are set in this simulation. The first step time is 0–8 s, and the tube is mainly assembled with the cam under the hydraulic pressure and finally the process of hydraulic pressure release and rebound. The second step is 9–12 s; the assembled camshaft is subjected to a torsion analysis under different conditions, and the torque is increased linearly with a maximum of 200 N·m in this FEA. Particularly, the setting of the torsion was important in the second step. Cams 1 and 3 were fixed, and cam 2 was torqued. First, a center point was created at the center of cam 2, and the center axis of the geometric model passed through the center point. Subsequently, the outer surface of cam 2 was coupled with its center point, i.e., a coupling relationship was established between the outer surface and the center point. Next, an appropriate spatial coordinate system *O-xyz* was established at the same center point of cam 2, and the torque about the center axis was applied to cam 2 (Figure 6b). Finally, the torsion angle θ of the cam was obtained by outputting the angular displacement of the center point in ABAQUS 6.14 software, as shown in Figure 6c. Furthermore, Standard/Explicit was used to analyze the model, which significantly saved the simulation time and improved the calculation accuracy.

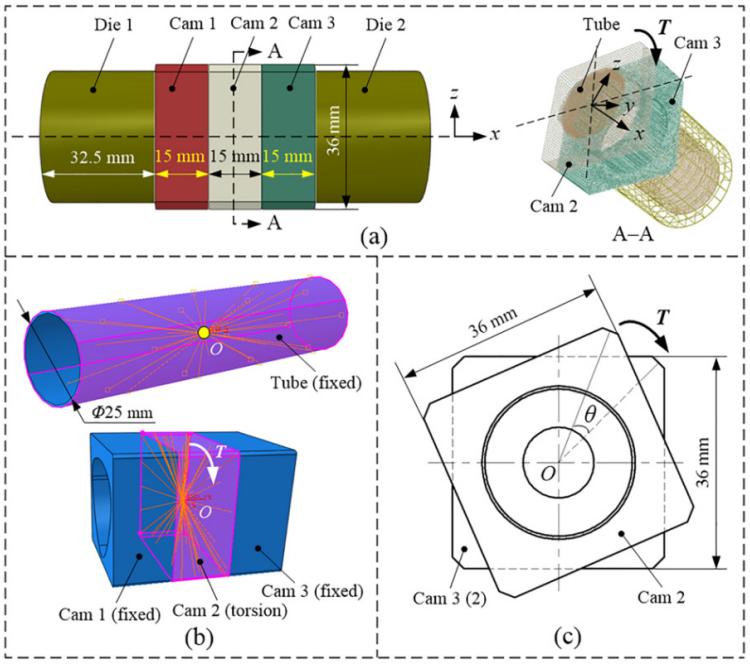

Figure 6. Assembled camshaft under pulsating hydraulic pressure [28]: (**a**) finite element model; (**b**) coupling setting of cam, shaft and center point and (**c**) torsion state.

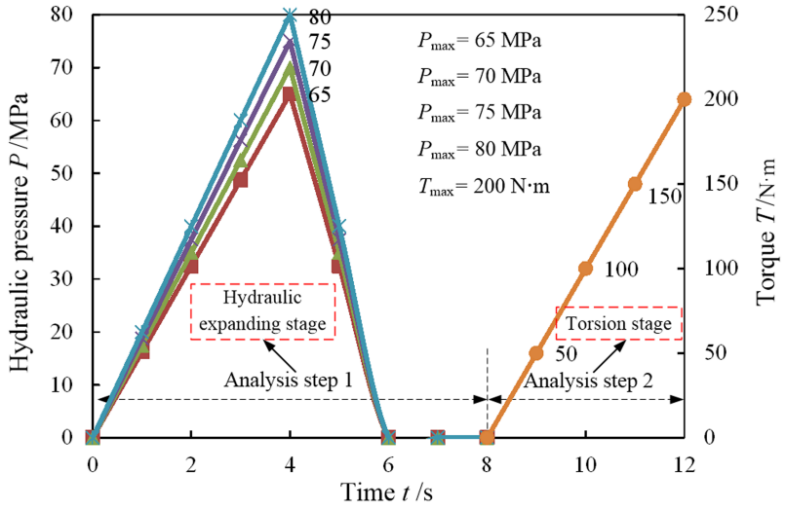

Figure 7. The loading curves adopted in this finite element simulation.

Furthermore, the basic size of all the components in the finite element model was set the same as that in the above experiments, as shown in Figure 6a. In this FEA, the mesh sizes of the tube and cam were 1 and 2 mm, respectively. The mesh type was hexahedral, and the element type was C3D8R. Symmetrical constraints were applied to dies 1, 2 and cams, whereas a free constraint was applied to the tube. The dies were set as rigid, and the tube and cam were set as deformable. Cams 1 and 3 were set as fixed constraints, i.e., cam 2 needed to be torqued in the second analysis step. The two dies were used to locate the two ends of the tube. The friction coefficient between the cam and the tube was 0.12, and that between the other components was 0.8. Table 6 lists the relevant parameters of FE model of hydraulically expanding assembled camshaft. Moreover, in ABAQUS 6.14 software, the point B in Figure 1b is selected to extract the residual contact pressure and shear stress under various conditions. The specific data are listed in Table 5.

Table 6. Relevant parameters of isometric-trilateral profile in ABAQUS 6.14 software.

Cross-Section Profile of cam-Bores	Hydraulic Pressure P_{max}/MPa	Mesh Quantity of Cams 1, 2 and 3	Mesh Quantity of Tube	Analysis Step
Isometric-trilateral profile	65, 70, 75, 80	11,415	20,956	2

4. Establishment of BP Neural Network Model

In this section, based on the analysis results of orthogonal torsion experiment, laser measurement experiment and finite element simulation, the BP neural network model which is most widely used in the artificial neural network is established. Through repeated training of the BP neural network samples, the network structure, transmission function, learning function, training function and error function are determined. A more accurate training model will be used to predict the main failure factors and further determine the failure manifestation of the assembled camshafts.

4.1. Basic Principles

As we all know, BP neural network is a multi-layer network model with multi-layer network learning algorithm and back-propagation [30]. The network has the advantages of complete structure, concise and easy to improve algorithm, strong nonlinear adaptability, highly autonomous learning and organizing ability, dynamic characteristics of learning and adapting uncertain system, strong robustness and fault tolerance, etc. It is the most widely used network model of artificial neural network in practical application and is most

suitable for solving complex and uncertain sum nonlinear problems. The general structure of the neural network is shown in Figure 8a.

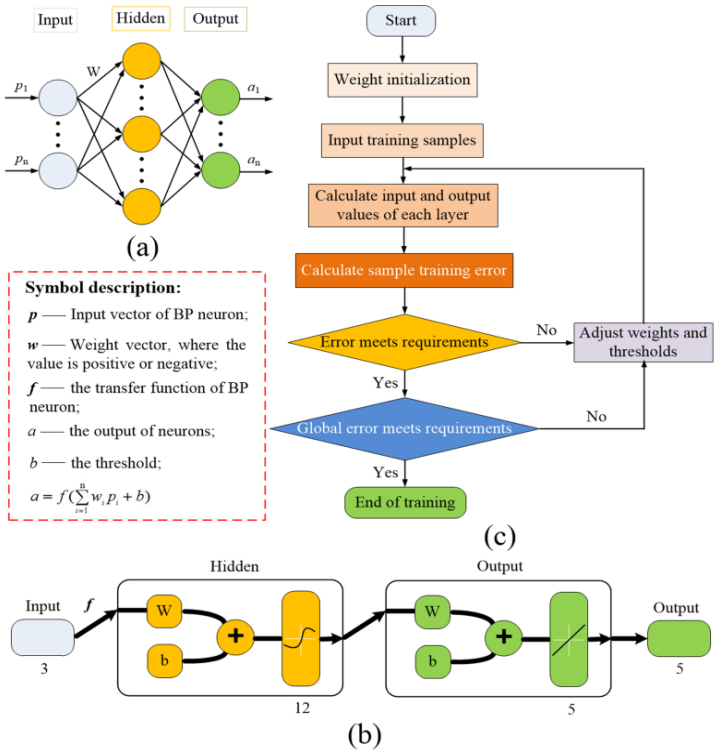

Figure 8. BP neural network: (**a**) single hidden layer, (**b**) network structure and (**c**) learning procedure.

4.2. Parameters Determination

In the process of constructing a BP neural network model, the structure of the BP neural network should be determined; that means to determine the number of hidden layers and corresponding nodes of the BP neural network. According to the previous experience, the number of hidden layer nodes can be designed according to Equation (4).

$$n = \sqrt{n_{\mathrm{i}} + n_{\mathrm{o}}} + a \tag{4}$$

where n, n_{i} and n_{o} represent the number of nodes in the hidden layer, input layer and output layer, respectively; a is the adjustment constant, which is usually selected between [1,10]. In this study, the BP neural network has only one hidden layer, and according to Equation (4), the number of hidden layer nodes is 12.

The *S*-type Tansig function (see Equation (5)) is selected as the transfer function between the input layer and the hidden layer of the BP neural network, and the linear Purelin function shown in Equation (6) is selected for the transfer function between the input layer and hidden layer of the BP neural network. The training function is Trainlm function, and the learning function is the default Learngdm function in MATLAB R2018b neural network toolbox. The error performance function is mean squared error (MSE). It is shown in Equation (7).

$$f(x) = \frac{1}{1 + e^{-x}} \tag{5}$$

$$f(x) = kx + c \tag{6}$$

$$mse = \frac{\sum_{k=1}^{n} (t_k - a_k)^2}{n} \tag{7}$$

In the above equations, n is the number of output units; c is a constant; a_k is the actual value of the k-th output unit; t_k is the expected value of the k-th output unit. In summary, the final BP neural network structure is shown in Figure 8b.

4.3. Learning Procedure

The learning of BP neural network is essentially the training of the BP algorithm, namely, learning and correcting the thresholds and weights of the neural network algorithm through a large number of test samples. It is an important process for establishing an accurate neural network model. The neural network toolbox in MATLAB automatically divides the data into two parts: training and testing, in the process of training the network. The specific learning and training steps are demonstrated in Figure 8c.

5. Results and Discussion

In this section, the accuracy of the BP neural network model is verified with the regression analysis method; then the main failure factors of the assembled camshaft are analyzed and predicted, and the error analysis of the predicted values of output parameters is performed. Then, the failure manifestations of assembled camshaft are displayed by the experiment from the microscopic perspective. Finally, the causes of failure are analyzed by using the minimum cut set in the FT theory; the weight distribution of the main events in the FT is given, and the specific measures to prevent failure are proposed.

5.1. Prediction of Main Failure Factors using BP Neural Network

The regression analysis method is used to quantitatively analyze the correlation between the training results of the neural network and the target value, which is described by the correlation coefficient R. Figure 9 shows the regression analysis results of training samples, test samples and all samples. The abscissa of each graph represents the target value, and the ordinate represents the output value, which is the training result. The range of correlation coefficient R is $[-1, 1]$, and the closer R is to ± 1, it indicates that the greater the correlation between the two variables, the higher the prediction accuracy of neural network. As illustrated in Figure 9a, the correlation coefficient R of the training sample reaches 0.99979, indicating that the training output value is almost identical to the target value. As illustrated in Figure 9b, the correlation coefficient R of the test sample is 0.99362, which is slightly lower than that of the training sample, but the verification result is still good. Figure 9c presents the final correlation coefficient R of all samples which is 0.99835. On the whole, the output value has a good correlation with the target value, and the prediction accuracy of the BP neural network is higher herein.

As demonstrated in Figure 10a, the network has been repeatedly trained. Finally, it is found that when the training reaches eight times, the training accuracy of the BP neural network has reached the maximum value, and the training stops automatically. At this time, the corresponding minimum mean square error is 0.0030455, which does not meet the requirement of 0.0001, but the training result is the best among the repeated training results. In addition, it can be seen from Figure 10b that the relevant parameters of the gradient descent algorithm used in the BP neural network changed in this study. The main failure factors of assembled camshafts are predicted by the trained BP neural network as follows.

Using the above training function as the BP neural network model after training, the last three groups of test samples shown in Table 5 are simulated. After the simulation, the output results of torque, surface roughness, scratch width, shear stress and residual contact pressure are displayed in the same picture as the target value in Figure 11. The output values corresponding to the 17 groups of samples are the results of training 17 groups of training samples with the BP neural network, and the output values of the last three groups of samples are the predicted output values obtained using simulation of the BP neural network obtained through training. The prediction results, target values and relative error values of three test samples, 18, 19 and 20, obtained using the BP neural network simulation are listed in Table 7. It can be seen from Table 7 that the maximum relative error of torque prediction value is -6.97%; the maximum relative error of surface roughness prediction value is 5.75%; the maximum relative error of scratch width prediction value is 8.34%; the maximum relative error of shear stress prediction value is -7.63%, and the maximum relative error of residual contact pressure prediction value is -6.61%. As a whole, the

fitting degree between the training results of the five output parameters and the target value can be obtained. The fitting degree of torque and scratch width is relatively poor, and the prediction accuracy of shear stress and residual contact pressure is higher. The prediction accuracy of all prediction results is more than 91%, and the highest prediction accuracy can reach 99.78%.

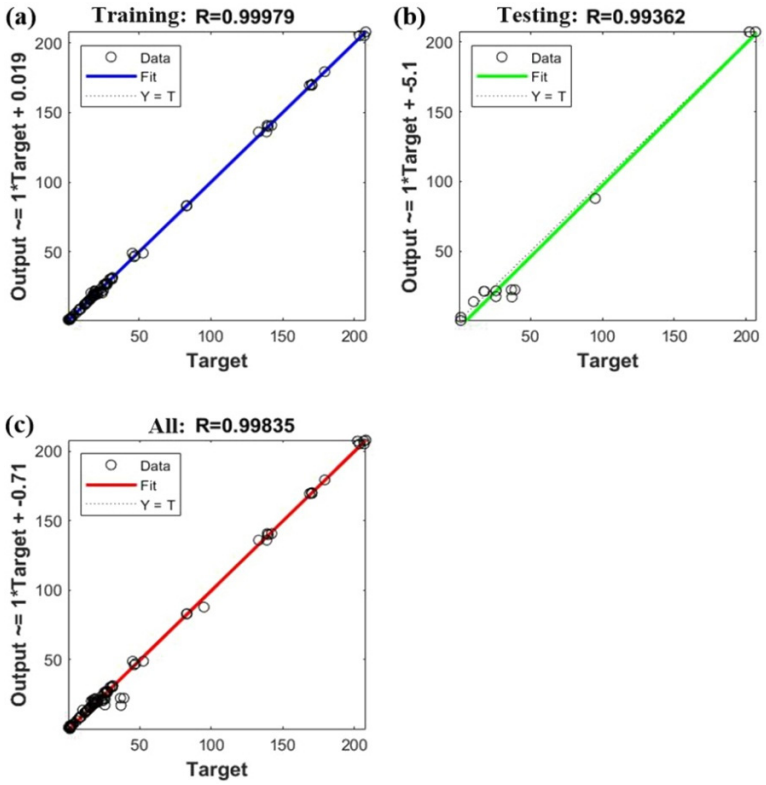

Figure 9. Regression analysis of BP neural network: (**a**) training samples, (**b**) testing samples and (**c**) all samples.

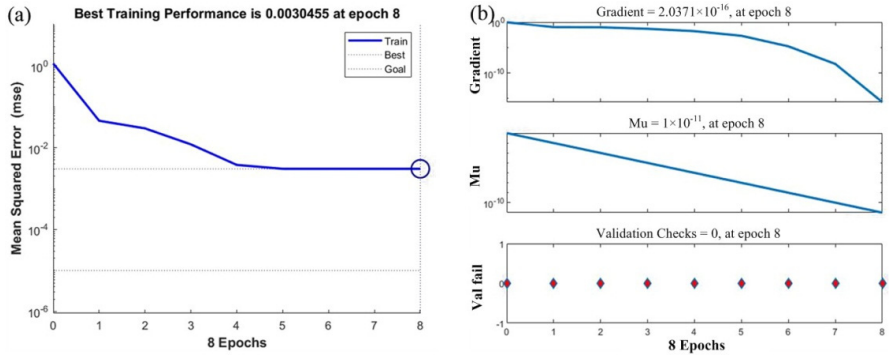

Figure 10. BP neural network: (**a**) mean square error and (**b**) gradient descent algorithm parameters.

5.2. Failure Manifestation of Assembled Camshaft

To see the partial failure manifestation more clearly and intuitively, a 2D microscopic image of the tubular outer surface was obtained with the OLYMPUS OLS4100 3D measuring laser microscope, as shown in Figure 12. After the orthogonal torsion experiment under different conditions, there are different degrees of scratches on the tubular outer surface. Most of these scratches are generated along the torsion direction; some are regular; some are disordered, and the width and depth of these scratches have a vital impact on the accumulation of surface damage. Once there are scratches on the tubular surface, the surface roughness changes accordingly, gradually accumulating and finally developing

surface damage, which causes the relative sliding between cam and tube and leads to the failure generation of the assembled camshaft.

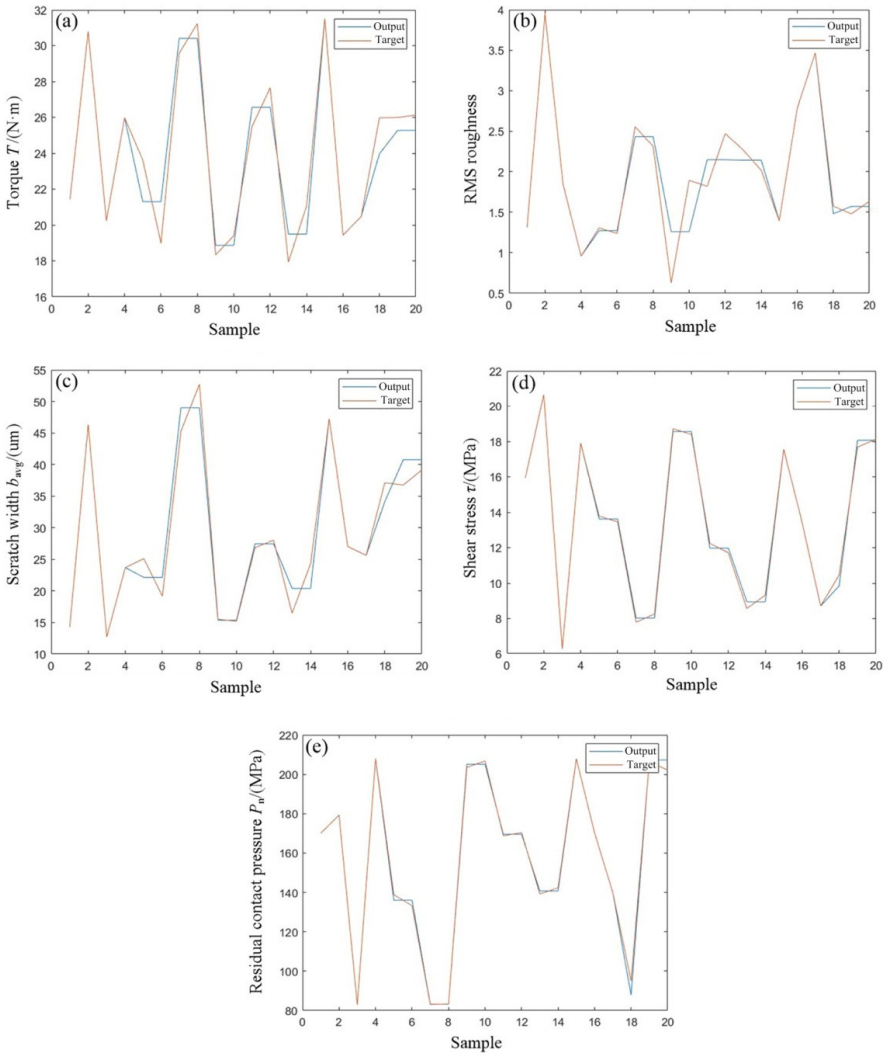

Figure 11. Output and target values of BP neural network: (**a**) torque, (**b**) surface roughness, (**c**) scratch width, (**d**) shear stress and (**e**) residual contact pressure.

Table 7. Predicted values and relative errors of three test samples.

No.	Output Parameters	Target Values	Predicted Values	Relative Errors (%)
18	Torque T/(N·m)	25.9765	24.1643	−6.97
18	Surface roughness R_q	1.573	1.496	−4.89
18	Scratch width b_{avg}/(um)	37.125	36.954	−0.46
18	Shear stress τ/(MPa)	10.4553	9.6566	−7.63
18	Residual contact pressure P_n/(MPa)	95.032	88.741	−6.61
19	Torque T/(N·m)	25.9894	25.4208	−2.18
19	Surface roughness R_q	1.478	1.563	5.75
19	Scratch width b_{avg}/(um)	36.758	39.825	8.34
19	Shear stress τ/(MPa)	17.6845	18.0052	1.81
19	Residual contact pressure P_n/(MPa)	206.519	206.972	0.22
20	Torque T/(N·m)	26.1291	25.4208	−2.71
20	Surface roughness R_q	1.633	1.612	−1.28
20	Scratch width b_{avg}/(um)	39.146	41.218	5.29
20	Shear stress τ/(MPa)	18.124	18.0465	−0.42
20	Residual contact pressure P_n/(MPa)	202.168	208.569	3.16

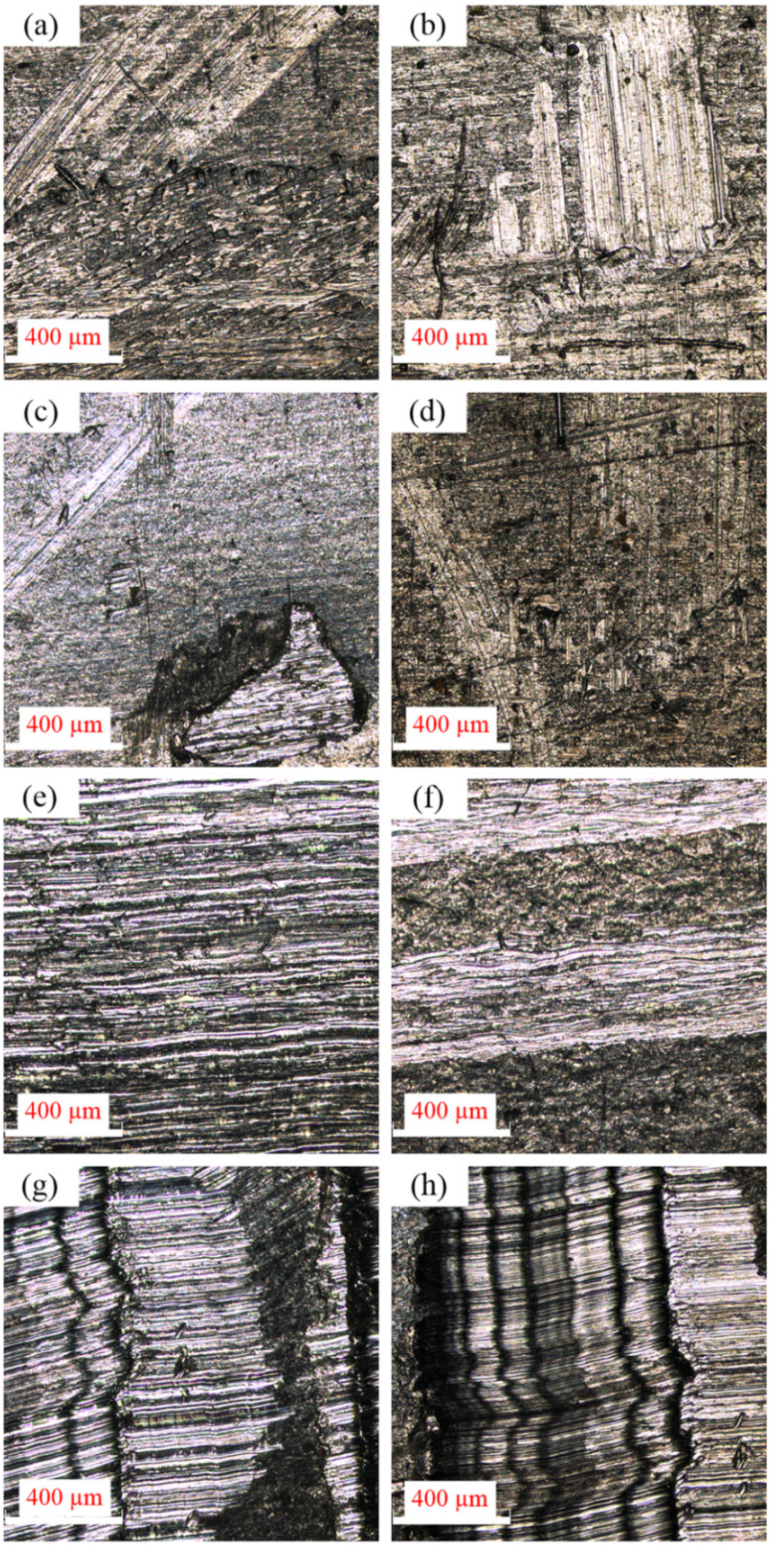

Figure 12. Micrograph of the tubular outer surface in assembled camshafts (**a**–**h**) [28].

In addition, there are pits, holes, distortion and excessive wear on the tubular surface as shown in Figure 12c,d,g,h. These failure manifestations affect the surface roughness of the tube, thus weakening the anti-torsion ability of the camshaft and resulting in the failure of the assembled camshaft which cannot be used normally.

The 3D failure manifestations of the outer surface of the tube in Figure 12a,c,e,g are displayed in Figure 13, and the failure manifestations of the assembled camshaft can be

observed more intuitively, that is, failures such as wear, scratch, damage, hole, pit and distortion on the tubular surface.

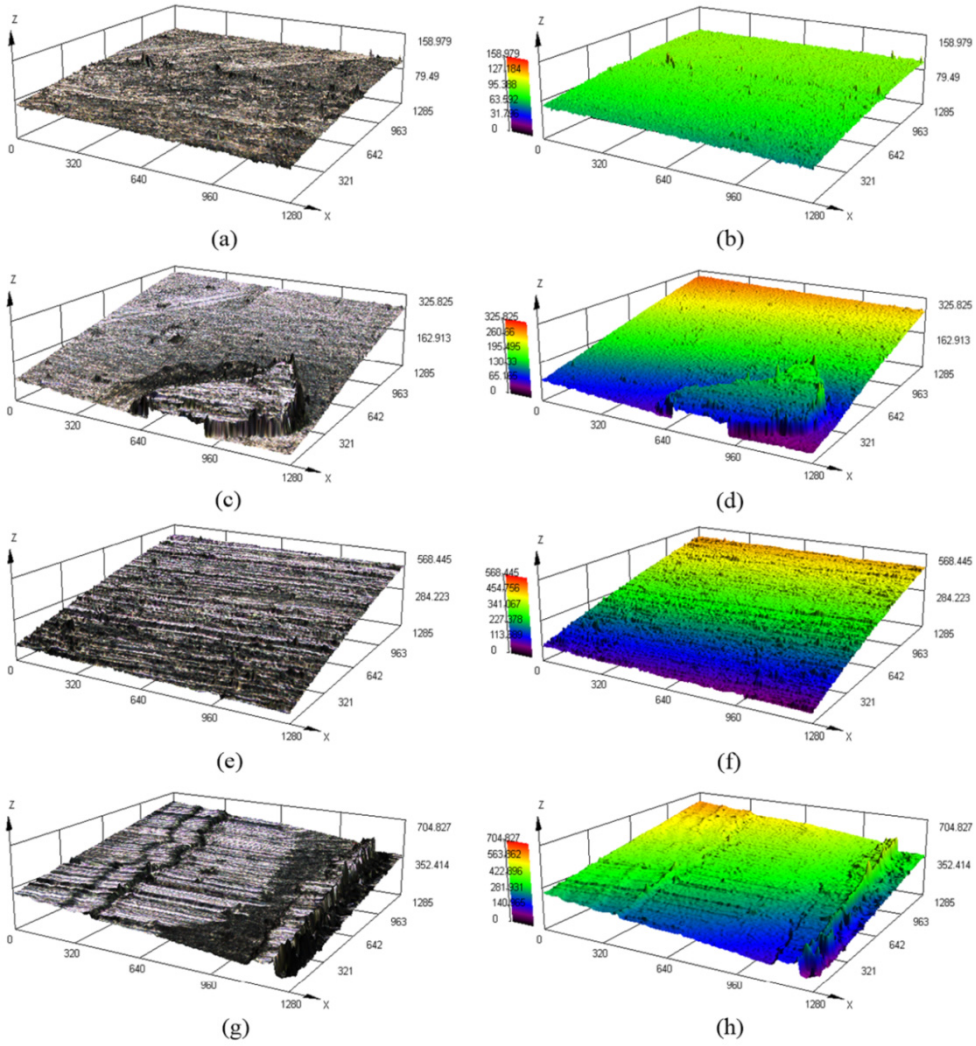

Figure 13. Topography of the tubular outer surface in the assembled camshafts (**a**–**h**).

5.3. Analyzing Failure Causes with Failure Tree Theory

Failure tree (FT) is a deductive failure analysis method from top to bottom. It is a deductive, structured methodology that is used to identify potential causes of a top event. It uses Boolean logic to combine low-order events to analyze the unwanted state in the system. It is mainly used in the field of safety engineering and reliability engineering to understand the cause of system failure and find the best way to reduce risk or to confirm the occurrence probability of a certain safety accident or specific system failure [31].

Fault tree analysis (FTA) uses the establishment of the logic diagram of the whole system to find the relationship among failure, subsystem and redundant safety design elements [32]. If there is a specific event in the result event, it affects multiple subsystems, and this is called common cause. From the perspective of graph, an event appears many times in the failure tree, and the common cause will bring about dependency among the events. The path from the initiator to the event is called cut set. The shortest path from the basic event to the event is called the minimum cut set, and the related calculation and analysis will be expanded in the Results and discussion. The failure tree model in this study is illustrated in Figure 14, and the relationships between events are described using gate symbols. The constructed FT model is useful for investigating the risks of the top event both qualitatively and quantitatively.

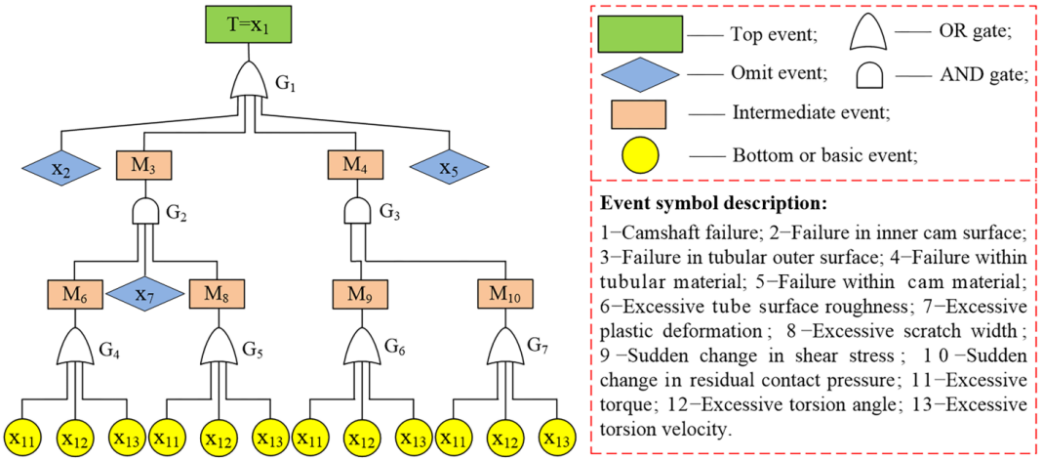

Figure 14. Failure tree model in this study, including the symbol description of each event and symbol of each logic gate.

Qualitatively, an expression is derived for the top event through the combinations of primary and basic events and using Boolean algebra. The qualitative evaluation of failure trees by the accounting of cut or path sets is conceptually simple. The OR gate logic in a tree represents the union set of input events. Similarly, the AND gate logic represents the product set of input events.

OR gate: as long as any one of the input events occurs, the output event occurs. If the input event is B_i (i = 1, 2, . . . , n), its logical relationship can be written as:

$$A = B_1 \cup B_2 \cup \ldots \cup B_n = \cup_{i=1}^{n} B_i \quad (8)$$

AND gate: only when all input events exist at the same time, the output event occurs. Assuming that the AND gate has n input events B_i (i = 1, 2, . . . , n), its logical relationship can be expressed as:

$$A = B_1 \cap B_2 \cap \ldots \cap B_n = \cap_{i=1}^{n} B_i \quad (9)$$

Quantitatively, the probability of the top event can be calculated from the primary and basic events regarding the minimal cut sets. The quantitative evaluation of failure trees can determine the probability of occurrence of the top event. To further determine the possible combined failure modes of assembled camshafts, based on the FT theory, the minimum cut set of the system is obtained. The expression of the minimum cut set can be obtained as:

$$T = G_1 = x_2 + G_2 + G_3 + x_5 \quad (10)$$

Then,

$$T = x_2 + G_4 x_7 G_5 + G_6 G_7 + x_5 \quad (11)$$

Further,

$$T = x_2 + (x_{11} + x_{12} + x_{13})(x_7)(x_{11} + x_{12} + x_{13}) + (x_{11} + x_{12} + x_{13})(x_{11} + x_{12} + x_{13}) + x_5 \quad (12)$$

According to the absorption law and idempotent law in Boolean algebra, the simplified results are as follows:

$$T = x_2 + {x_{11}}^2 x_7 + {x_{12}}^2 x_7 + {x_{13}}^2 x_7 + 2x_{11}x_{12}x_7 + 2x_{11}x_{13}x_7 + 2x_{12}x_{13}x_7 + {x_{11}}^2 + {x_{12}}^2 + {x_{13}}^2 + 2x_{11}x_{12} + 2x_{11}x_{13} + 2x_{12}x_{13} + x_5 \quad (13)$$

Thus, the minimum cut sets in the FT of the assembled camshaft are as follows: {x_2}, {x_5}, {x_{11}}, {x_{12}}, {x_{13}}, {x_7, x_{11}}, {x_7, x_{12}}, {x_7, x_{13}}, {x_{11}, x_{12}}, {x_{11}, x_{13}}, {x_{12}, x_{13}}, {x_7, x_{11}, x_{12}}, {x_7, x_{11}, x_{13}} and {x_7, x_{12}, x_{13}}. There are 14 minimum cut sets in the FT, and 14 possible top events. The basic events x_{11}, x_{12} and x_{13} are common causes, that is, it will have complex effects on multiple subsystems. For example, x_{11}, x_{12} and x_{13} affect M_6 and M_8,

namely, torque, torsion angle and torsion velocity affect surface roughness and scratch width, respectively. In addition, the weight distribution of the major events (main failure factors) is shown in Figure 15.

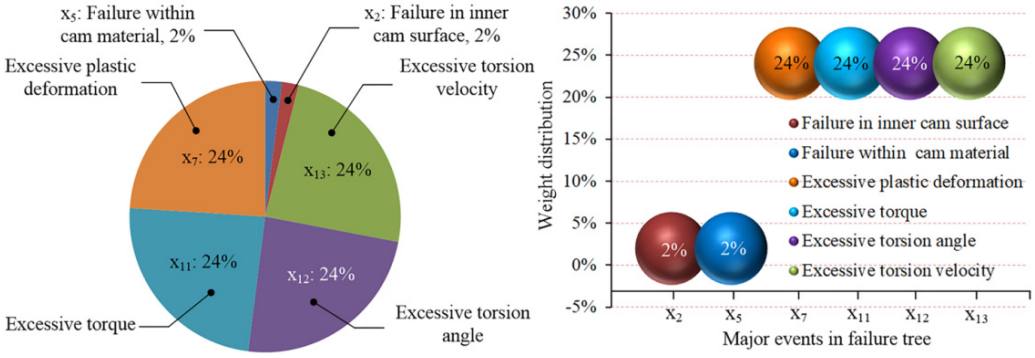

Figure 15. Weight distribution of major events in failure tree of assembled camshaft.

As demonstrated in Figure 15, the probability of occurrence of the basic events x_{11}, x_{12} and x_{13} is 24%. Since the basic event is the common cause of the system, it has a complex impact on the above intermediate events, and the probability of occurrence is high. The probability of occurrence of omit events x_2 and x_5 is 2%, which is not considered by the system for the moment, while the probability of omit event x_7 is as high as 24%, which is caused by the repeated occurrence of event x_7 when calculating the minimum cut set. Furthermore, event x_7 represents the excessive plastic deformation of the tube, which is not obvious in this system, so it is not considered as the main factor at present. Namely, torque, torsion angle and torsion velocity will have certain influence on the surface roughness, scratch width, shear stress and residual contact pressure, corresponding to the outer surface damage of tubular material and the internal damage of material, respectively; the failure or damage of cam surface and material itself will not be considered. During torsion, due to the different torque, torsion velocity and torsion angle, the tubular outer surface will be scratched, and the surface roughness will change under the interaction of basic events x_{11}, x_{12} and x_{13}. When the basic events x_{11}, x_{12} and x_{13} reach a certain value, the shear stress and residual contact pressure between the tube and cam contact interface change suddenly. From the view of mechanics, it can be concluded that the failure of camshaft has occurred at this time. That is, the failure of the assembled camshaft is affected by many factors, which are interrelated.

Therefore, in the actual application of camshafts, a series of measures, such as reasonably matching the engine velocity, timely adjusting the operating cycle and torsional angle and appropriately adding lubricant to reduce friction and wear, are necessary to prevent the failure of hydraulic expanding assembled camshafts.

6. Conclusions

In this study, a more accurate BP neural network model is constructed to predict the main failure factors of the hydraulic expanding assembled camshafts. The failure manifestations of the assembled camshaft are displayed. The causes of failure are analyzed by using the minimum cut set in the FT theory; the weight distribution of the main events is provided, and the specific measures to prevent failure are proposed from a macro perspective. The main conclusions of this study are as follows:

(1) A BP neural network method for predicting the main failure factors of hydraulic expanding assembled camshafts is proposed. The correlation between the training results of the neural network and the target value is quantitatively analyzed by using the regression analysis method, and the accuracy of the BP neural network model is verified. The research shows that the accuracy of the BP neural network model is good, and the prediction accuracy of all results is more than 91%, of which the highest prediction accuracy can reach 99.78%.

(2) The failure manifestations of assembled camshaft mainly include wear, scratch, damage, hole, pit and distortion on the tubular surface. The FT model of the assembled camshaft is constructed; the minimum cut set of the camshaft system is calculated by using the FT theory, and the causes of the failure of the assembled camshaft are analyzed. The more minimum cut sets, the more dangerous the assembled camshaft system.

(3) During torsion, due to factors such as different torsion force, torsional angle and torsion velocity, the tubular surface is excessively worn, which changes the frictional characteristics (surface roughness) between the cam and the tube and causes the shear stress and residual contact pressure to change abruptly. Further, relative sliding occurs between the tube and the cam, resulting in the failure of the assembled camshafts.

Because some data in this study are not easy to obtain, the data used come from the two parts of experiment and simulation, which may lead to some errors. Certainly, to reduce the error, the experiment and simulation conditions are set to be identical as far as possible in this study. In addition, there are few systematic studies on the failure of the novel hydraulic expanding assembled camshafts. We believe that this study can provide some guidance and reference value for the follow-up work, the actual industrial production, failure prevention, faults monitoring and performance improvement of hydraulic expanding assembled camshafts in the future.

Author Contributions: Conceptualization, J.M. and L.Y.; data curation, J.M. and L.S.; formal analysis, J.M. and S.P.; funding acquisition, L.Y.; investigation, J.M., Z.G. and H.H.; methodology, J.M.; project administration, L.Y.; resources, J.M. and L.Y.; supervision, L.Y.; validation, J.M., L.S., Z.G., S.P. and H.H.; writing—original draft, J.M.; writing—review and editing, J.M. and L.Y. All authors have read and agreed to the published version of the manuscript.

Funding: This research was funded by the National Natural Science Foundation of China (52065014), Natural Science Foundation of Guangxi Province (2017GXNSFAA198133), Guangxi Key Laboratory of Manufacturing System & Advanced Manufacturing Technology, Guilin University of Electronic Technology (22-35-4-S013, Guilin 541004, China) and Innovation Project of Guangxi Graduate Education (JGY2019074).

Institutional Review Board Statement: Not applicable.

Informed Consent Statement: Not applicable.

Data Availability Statement: Not applicable.

Conflicts of Interest: The authors declare no conflict of interest.

References

1. Horvat, G.L.; Surface, S.C. Assembled Camshafts for Automotive Engines. *J. Mater. Shap. Technol.* **1989**, *7*, 133–136. [CrossRef]
2. Scherzer, R.; Fritsch, S.; Landgraf, R.; Ihlemann, J.; Franz, M.W.X. Finite Element Simulation of the Presta Joining Process for Assembled Camshafts: Application to Aluminum Shafts. *Metals* **2018**, *8*, 128. [CrossRef]
3. Meusburger, P. The Camshaft as an Example of Lightweight Design in Engine Construction. *ThyssenKrupp Techforum* **2004**, *12*, 50–55.
4. Lin, B.J.; Yu, G.; Yang, S.H.; Kou, S.Q.; Wang, J.H. Application of a New Type Feedforward-Feedback Controller in Assembly Machine for Assembled Camshaft. *Assem. Autom.* **2012**, *32*, 333–339. [CrossRef]
5. Chen, J.T.; Yang, L.F. State-of-the-art of Joining Technologies for Assembled Camshaft. *Adv. Mater. Res.* **2013**, *602–604*, 2118–2122. [CrossRef]
6. Ma, J.P.; Yang, L.F.; He, Y.L. Dynamic Frictional Characteristics of TP2 Copper Tubes during Hydroforming under Different Loading and Fluid Velocities. *J. Mater. Eng. Perform.* **2019**, *28*, 3661–3672. [CrossRef]
7. Hwang, Y.M.; Manabe, K.I. Latest Hydroforming Technology of Metallic Tubes and Sheets. *Metals* **2021**, *11*, 1360. [CrossRef]
8. Zhang, J.; Li, H.Y.; Li, H.; Jia, H. Investigation on Fatigue Performance of Adhesively Bonded Butt-joints and Multiaxial Life Estimation Using Stress-based Failure Models. *Theor. Appl. Fract. Mech.* **2020**, *107*, 102498. [CrossRef]
9. Yanarocak, R.K.; Boz, H. Design Optimization of a Valvetrain System under Engine Brake Switch Loading by Means of Strain Measurement. *SAE Int. J. Eng.* **2016**, *9*, 1825–1832. [CrossRef]
10. Singh, S.S.K.; Abdullah, S.; Nikabdullah, N. The Needs of Understanding Stochastic Fatigue Failure for the Automobile Crankshaft: A Review. *Eng. Fail. Anal.* **2017**, *80*, 464–471. [CrossRef]
11. Ktari, A.; Haddar, N.; Ayedi, H.F. Fatigue Fracture Expertise of Train Engine Crankshafts. *Eng. Fail. Anal.* **2011**, *8*, 1085–1093. [CrossRef]

12. Becerra, J.A.; Jimenez, F.J.; Torres, M.; Sanchez, D.T.; Carvajal, E. Failure Analysis of Reciprocating Compressor Crankshafts. *Eng. Fail. Anal.* **2011**, *18*, 735–746. [CrossRef]
13. Liu, Y.; Mahadevan, S. Stochastic Fatigue Damage Modeling under Variable Amplitude Loading. *Int. J. Fatigue* **2007**, *29*, 1149–1161. [CrossRef]
14. Ling, Y.; Shantz, C.; Mahadevan, S.; Sankararaman, S. Stochastic Prediction of Fatigue Loading Using Real-time Monitoring Data. *Int. J. Fatigue* **2011**, *33*, 868–879. [CrossRef]
15. Jeon, W.S.; Song, J.H. An Expert System for Estimation of Fatigue Properties of Metallic Materials. *Int. J. Fatigue* **2002**, *24*, 685–698. [CrossRef]
16. Wang, G.; Taylor, D.; Bouquina, B.; Devlukiab, J.; Ciepalowicz, A. Prediction of Fatigue Failure in a Camshaft Using the Crack Modelling Method. *Eng. Fail. Anal.* **2000**, *7*, 189–197. [CrossRef]
17. Ossai, C.I.; Boswell, B.; Davies, I. Markov Chain Modelling for Time Evolution of Internal Pitting Corrosion Distribution of Oil and Gas Pipelines. *Eng. Fail. Anal.* **2016**, *60*, 209–228. [CrossRef]
18. Nipane, R.D.; Patil, R.K. Modelling and Fatigue Analysis of Metal Matrix Composite Camshaft Using Finite Element Analysis. *Int. Eng. Res.* **2015**, *1*, 497–501.
19. Zhai, Z.F.; Yang, L.F. Joint Structure between the Shaft and Cam Lobes in Assembled Camshaft. *Adv. Eng. Res.* **2015**, *9*, 274–277.
20. Zhai, Z.F.; Yang, L.F.; Ma, J.P.; Zhang, M.H. An Evaluation of the Assemblability of Two Novel Assembled Camshaft Configurations by Tube Hydroforming. In Proceedings of the Esaform2017, Dublin, Ireland, 26–28 April 2017. AIP Conference Proceedings.
21. Qiao, J.; Kou, S.Q.; He, D.Y.; Yang, S.H. Torque Strength and Influencing Factors Analysis for Assembled Camshaft by Knurling Joining. *Mater. Sci. Forum* **2008**, *575–578*, 216–221. [CrossRef]
22. Londhe, A.; Yadav, V.; Patil, A. Evaluation of a 4-stroke 4-cylinder Diesel Engine Valve-train for Replacement of a Solid Camshaft with a Hollow Camshaft. *SAE Int. J. Engines* **2009**, *2*, 254–262. [CrossRef]
23. Dong, T.; Wang, H.J.; Shi, L. Study of Camshaft Grinders Faults Prediction Based on RBF Neural Network. *Appl. Mech. Mater.* **2012**, *141*, 519–523. [CrossRef]
24. Yang, M.S.; Kong, X.J.; Gao, X.Q.; Liu, Y.; Li, Y. FOA Based Diagnosis Model for Multivariate Production Process. *Int. J. u- e-Serv. Sci. Technol.* **2015**, *8*, 347–356. [CrossRef]
25. Li, Z.; Jiang, Y.; Duan, Z.; Peng, Z. A New Swarm Intelligence Optimized Multiclass Multi-kernel Relevant Vector Machine: An Experimental Analysis in Failure Diagnostics of Diesel Engines. *Struct. Health Monit.* **2018**, *17*, 1503–1519. [CrossRef]
26. Czyzewski, T.; Odman, M.T. Analysis of Contact Stress and Deformation in a Trilobe Polygonal Connection. *J. Manuf. Sci. Eng.* **1988**, *110*, 212–217. [CrossRef]
27. Kahn-Jetter, Z.L.; Hundertmark, E.; Wright, S. Comparison of Torque Transmitting Shaft Connectivity using a Trilobe Polygon Connection and an Involute Spline. *J. Mech. Des.* **2000**, *122*, 130–135. [CrossRef]
28. Ma, J.P.; Yang, L.F.; Liu, J.; Chen, Z.B.; He, Y.L. Evaluating the Quality of Assembled Camshafts under Pulsating Hydroforming. *J. Manuf. Process.* **2021**, *61*, 69–82. [CrossRef]
29. Ma, J.P.; Yang, L.F.; Huang, J.J.; Chen, Z.B.; He, Y.L.; Jiang, J.Y. Residual Contact Pressure and Elastic Recovery of an Assembled Camshaft using Tube Hydroforming. *CIRP J. Manuf. Sci. Technol.* **2021**, *32*, 287–298. [CrossRef]
30. Gao, G.Y.; Zhang, Z.; Cai, C.; Zhang, J.L.; Nie, B.H. Cavitation Damage Prediction of Stainless Steels Using an Artificial Neural Network Approach. *Metals* **2019**, *9*, 506. [CrossRef]
31. Mohammad, Y.; Farzaneh, N.; Mahnaz, N. Failure Probability Analysis by Employing Fuzzy Fault Tree Analysis. *Int. J. Syst. Assur. Eng. Manag.* **2017**, *8*, 1177–1193.
32. Qi, B.; Sun, X.M.; Liu, B.J.; Wu, X.; Gao, R.T.; Zhu, H.; Li, Y.H. Influencing Factors of Agricultural Machinery Accidents Based on Fuzzy Fault Tree Analysis. *J. Comput. Methods Sci. Eng.* **2022**, *22*, 871–881. [CrossRef]